Implementation and Validation of EXSIM (A Stochastic Finite-Fault Ground-Motion Simulation Algorithm) on the SCEC Broadband Platform

Article *in* Seismological Research Letters · January 2014

DOI: 10.1785/0220140097

CITATIONS
26

READS
1,665

2 authors:

Gail M. Atkinson
The University of Western Ontario
274 PUBLICATIONS **11,336** CITATIONS
SEE PROFILE

Karen Assatourians
The University of Western Ontario
37 PUBLICATIONS **381** CITATIONS
SEE PROFILE

Implementation and Validation of EXSIM (A Stochastic Finite-Fault Ground-Motion Simulation Algorithm) on the SCEC Broadband Platform

by Gail M. Atkinson and Karen Assatourians

Online Material: Input files for running EXSIM.

INTRODUCTION

This article describes the validation exercise associated with preparing EXSIM, a stochastic extended finite-fault algorithm for ground-motion simulation, for use as a time-history simulation module on the Southern California Earthquake Center (SCEC) Broadband Platform (BBP), version 14.3. This involved importing the algorithm to the SCEC computational platform and standardization and calibration of the input parameters. Herein, we (1) provide a brief overview of the EXSIM method of simulating time histories, (2) summarize its input parameters and their assigned values for generic applications in eastern and western North America (ENA and WNA, respectively), and (3) show comparisons of response spectra from EXSIM simulations with those of selected earthquake suites and ground-motion prediction equations (GMPEs).

EXSIM METHODOLOGY

EXSIM is an open-source stochastic finite-source simulation algorithm, written in FORTRAN, that generates time series of ground motion for earthquakes (Motazedian and Atkinson, 2005; Boore, 2009; Assatourians and Atkinson, 2012). A fault plane, having a specified size according to its seismic moment, is divided into an array of subsources, each of which is treated as a point source. Time series from the subsources are modeled using the point-source stochastic model developed by Boore (1983, 2003) and popularized by the Stochastic-Method SIMulation (SMSIM) computer code (Boore, 2003, 2005). The ground motion from each subsource is treated as random Gaussian noise of a specified duration, having an underlying spectrum as given by the Brune (1970, 1971) point-source model for shear radiation. The Brune model specifies the Fourier spectrum at the source by seismic moment and stress parameter and is attenuated in the frequency domain according to an empirical attenuation model. The duration of motion for each subsource comes from the source duration plus the path duration. The time series from the subsources are summed in the time domain, with appropriate time delays for propagation of the rupture front.

There have been several versions of stochastic finite-fault models upon which EXSIM was built (Beresnev and Atkinson, 1997; Motazedian and Atkinson, 2005; Boore, 2009; Assatourians and Atkinson, 2012). The version of EXSIM implemented in the broadband platform is that described by Assatourians and Atkinson (2012) and includes the improvements to the treatment of low frequencies proposed by Boore (2009), as well as the suggested switch from the normalization of high-frequency amplitudes based on velocity (as implemented in Motazedian and Atkinson, 2005) to an equivalent normalization based on acceleration (as suggested by Boore, 2009). Several cosmetic changes in input/output formats were also made to facilitate implementation of EXSIM on the broadband platform and to standardize input parameters. It is important to recognize that EXSIM is a simplistic model that aims to capture salient finite-fault effects from a geometric perspective only, without attempting to model details of the physics of rupture generation or propagation. In the broadband platform implementation of EXSIM, the option to inject deterministic coherent pulses (as described by Motazedian and Atkinson, 2005) is not used, as the aim is to model only those aspects of a rupture scenario that can be specified in advance (such as basic fault geometry).

Stochastic Point-Source Model for Subsources

Each subsource along the fault plane is modeled as a stochastic point source. The stochastic point-source model assumes that the source process is concentrated at a point and that the acceleration time series radiated to a site carry deterministic and random aspects of ground-motion shaking. The deterministic aspects are specified by the average Fourier spectrum, given as a function of magnitude and distance. The stochastic aspects are

doi: 10.1785/0220140097

treated by modeling the motions as Gaussian noise with the specified underlying spectrum. The steps of synthesizing ground motions for each subsource follow the methodology implemented in the SMSIM algorithm of Boore (2005):

1. Generate a normally distributed random signal having zero mean and unit variance.
2. Multiply the noise signal by a window function of specified duration; we use the Saragoni and Hart (1974) exponential window (with window parameters $W_\varepsilon = 0.2$ and $W_\eta = 0.2$).
3. Calculate the Fourier transform of the windowed signal.
4. Normalize the result so that the root mean square amplitude spectrum of the noise signal equals unity.
5. Calculate the theoretical (deterministic) point-source spectrum as a function of frequency (f), based on seismic moment (M_0) and distance from the point source (R):

$$A(M_0;R;f) = S(M_0;f)P(R;f)\text{Site}(f), \tag{1}$$

in which $A(M_0;R;f)$ is the Fourier spectrum of acceleration observed at the recording site, $S(M_0;f)$ is the source spectrum at unit distance, $P(R;f)$ is the path effect that includes the effects of both geometrical spreading and anelastic attenuation, and $\text{Site}(f)$ is the site-response operator. The source spectrum follows the Brune model (see Boore, 2003),

$$S(f) = \frac{CM_0 4\pi^2 f^2}{1+\frac{f^2}{f_0^2}}, \tag{2}$$

in which C is a constant, M_0 is the source moment, f is frequency, and f_0 is the corner frequency, related to the stress-drop parameter by

$$f_0 = 4.9\times 10^6 \beta \left(\frac{\Delta\sigma}{M_0}\right)^{\frac{1}{3}}, \tag{3}$$

in which β is shear-wave velocity in the source region in kilometers per second, $\Delta\sigma$ is the stress parameter in bars, and M_0 is in dyne·cm (Boore, 2003). The spectrum is attenuated with distance using an empirical attenuation operator. The user may choose a variety of attenuation shapes (linear, hinged-bilinear, hinged-trilinear), with the simplest being a linear model of the form

$$P(f) = \frac{e^{-\gamma(f)R}}{R}, \tag{4}$$

in which R is hypocentral distance and $\gamma(f)$ is anelastic attenuation, inversely related to the quality factor Q as

$$\gamma(f) = \frac{\pi f}{Q\beta}. \tag{5}$$

The site amplification operator $\text{Site}(f)$ is specified by the user to model the net effects of site amplification. This typically includes two components: (1) amplification through the regional crustal velocity gradient and (2) any high-frequency deamplification effects from near-surface materials, such as those characterized by $f_{\max}$ (Hanks, 1982) or kappa (Anderson and Hough, 1984).

6. Multiply equation (1) by the normalized (unit amplitude) noise spectrum.
7. Calculate the inverse Fourier transform of the site spectrum to obtain the simulated accelerogram.

The seven steps listed above produce a random-phase time series at an observation point for a specified point source at a specified distance.

Stochastic Finite-Source Modeling

There are important factors that influence the ground motions from large earthquakes that are not included in the stochastic point-source model, such as the effects of faulting geometry, distributed rupture, and rupture inhomogeneity. To consider these finite-fault effects in ground-motion modeling, Hartzell (1978) proposed subdividing the fault surface of an earthquake into a grid of subsources, each of which could be treated as a point source. The contributions to ground motion can be summed at the observation site, over all of the subsources comprising the fault, considering proper delays of subsources due to rupture propagation. This basic idea has been implemented in many articles (e.g., Irikura, 1983, 1992; Schneider *et al.*, 1993; Irikura and Kamae, 1994; Atkinson and Silva, 1997; Bour and Cara, 1997; Beresnev and Atkinson, 1998; Motazedian and

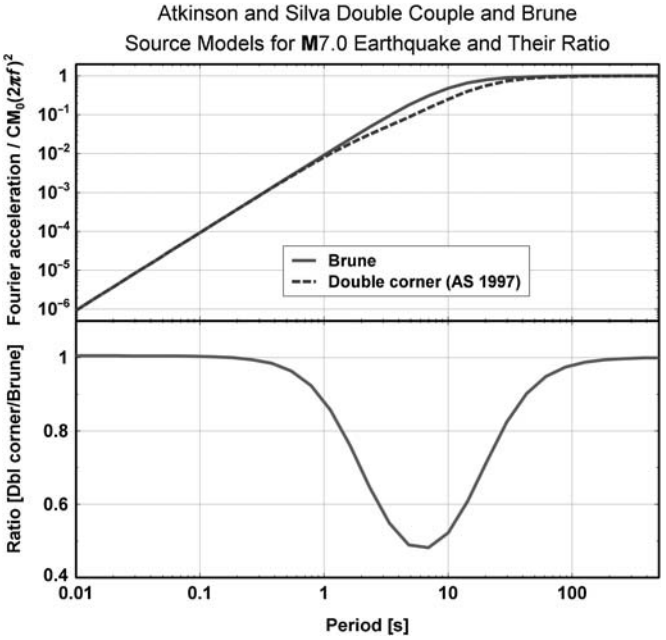

▲ **Figure 1.** (Top) The single (solid line) and double-corner (dashed line) source spectra for an M 7 earthquake. (Bottom) An empirical filter, derived as the ratio of the Brune model spectrum to the double-corner model spectrum, as specified by Atkinson and Silva (1997).

Atkinson, 2005; Boore, 2009). The implementation of this concept in EXSIM follows that described by Motazedian and Atkinson (2005), who introduced the concept of dynamic corner frequency. Their implementation had a significant advantage over previous algorithms in that it made the simulation results relatively insensitive to subsource size (as long as subsources are not smaller than ~1.5 km or are so big as to introduce discretization to simulated time series) and eliminated the need for multiple triggering of subevents. Boore (2009) further improved the algorithm, with modifications to the subevent normalization procedures that eliminated the remaining dependency on subsource size and improved the treatment of low-frequency amplitudes. He also pointed out that using a normalization scheme based on acceleration spectra (rather than velocity spectra) was advantageous in allowing consistent treatment of subsources between EXSIM and SMSIM. In the revised EXSIM algorithm, properly normalized and delayed subsource contributions are summed in the time domain as

$$A(t) = \sum_{i=1}^{N} H_i \times Y_i(t - \Delta t_i - T_i) \tag{6}$$

and

$$H_i = \frac{M_0}{M_{0_i}} \sqrt{\frac{\sum_j \left(\frac{f_0^2 f_j}{f_0^2 + f_j^2}\right)^2}{N \sum_j \left(\frac{f_{0_i}^2 f_j}{f_{0_i}^2 + f_j^2}\right)^2}}, \tag{7}$$

in which $A(t)$ is the total seismic signal at site, incorporating delays between subsources; H_i is a normalization factor for the ith subsource that aims to conserve high-frequency amplitudes; $Y_i(t)$ is the signal of the ith subsource (inverse Fourier transform of the subsource spectrum); N is the total number of subsources; Δt_i is delay time of the subsource; and T_i is a fraction of rise time. M_0 is the total seismic moment and M_{0i} is the

-Source:

- Magnitude: platform-specified
- Fault geometry, hypocenter: platform-specified
- Slip model: random
- Slip model seed: platform-specified
- Subsource size: 3.6 km × 3.5 km
- **Stress parameter:** 150 bars
- Subsource window: Saragoni–Hart ($W_\varepsilon = 0.2$, $W_\eta = 0.2$)
- V_{rup}/V_S : 0.8
- Risetime: $1/f_0$ (~inverse of subsource corner frequency)
- Pulsing%: 50%
- **Subsource duration (distance dependent):** $t = \begin{cases} 1 + 0.18 \times R & R \le 50 \text{ km} \\ 10 + 0.05 \times (R\text{-}50) & R > 50 \text{ km} \end{cases}$
- **Empirical double-corner filter:** applied
- H normalization: by acceleration

-Path:

- **Geometrical spreading**: $G(R) = \begin{cases} R^{-1} & R \le 40 \text{ km} \\ R^{-0.5} & R > 40 \text{ km} \end{cases}$
- **Anelastic attenuation**: $Q(f) = \max(150, 187 f^{0.55})$
- Shear-wave velocity: $\beta = 3.7$ km/s
- Density: 2.8 gm/cm^3

-Site:

- **Site and crustal amplification:** Atkinson and Boore (2006) spectral amplification model for 863 m/s, adjusted to apply to $V_S = 760$ m/s
- **Kappa**: platform-specified ($\kappa = 0.04$ s)

▲ **Figure 2.** Input parameters applied for California.

seismic moment of the ith subsource, which is calculated internally by EXSIM based on subsource size. (The user inputs the total moment of the earthquake and EXSIM calculates M_{0i} as the appropriate fraction of the total moment. In the BBP implementation, each realization adopts a random slip, and EXSIM uses the slip of each subsource to find M_{0i}, by multiplying the ratio of subsource slip to total moment by the sum of all subsource slips.) Following the same notation, f_0 is the corner frequency of the whole event, and f_{0i} is the corner frequency of the ith subsource (to be calculated using equation 8), whereas j is a counter over frequency. The rise time of each subsource in EXSIM is based on the subfault radius divided by the rupture velocity, whereas the total duration of radiation from the source will be controlled by the time required for rupture propagation along the length of the fault, as each subsource ruptures in turn and is then delayed accordingly in its arrival at the observation point. EXSIM considers the concept of self-healing along the fault in a very limited way, by allowing the user to specify the maximum percentage of the fault that may be active at a time; this is referred to as the pulsing% (see Motazedian and Atkinson, 2005, for details.)

The duration of radiation from the source in EXSIM does not depend explicitly on the stress parameter but may be implicitly dependent on the stress parameter if fault size depends on stress drop. For example, in Atkinson and Boore (2006), small faults were specified for eastern North America due to the high stress drop, thus resulting in relatively short source durations. In general, the treatment of source effects in EXSIM is simplistic and does not include the possible effects of factors such as source mechanism, depth, and so on, except indirectly through the ability to vary the stress parameter.

EXSIM INPUT PARAMETERS

Source Parameters, $S(f)$

The fault is modeled as a rectangular plane having specified dimensions (in kilometers), azimuth, and dip (in degrees). In the implementation of EXSIM on the BBP, the fault length and width are specified by the platform, using fault sizes consistent with the specified moment magnitude, according to the empirical relations of Leonard (2010). The relative amount of high-frequency energy from the source is governed by the stress parameter, which is input by the user then used by EXSIM (equation 2) in defining the subsource spectrum. Modifications to the source spectrum can be made by the user by specifying an additional empirical filter (a frequency-dependent amplification function), which is described further below. A source-effect filter and a site-effect filter are equivalent in EXSIM, in

-Source:	
• Magnitude:	platform-specified
• Fault geometry, hypocenter:	platform-specified
• Slip model:	random
• Slip model seed:	platform-specified
• Subsource size:	3.0 km × 3.0 km
• **Stress parameter:**	150 bars
• Subsource window:	Saragoni–Hart ($W_\varepsilon = 0.2$, $W_\eta = 0.2$)
• V_{rup}/V_S :	0.8
• Risetime:	$1/f_0$ (~inverse of subsource corner frequency)
• Pulsing%:	50%
• **Subsource duration (distance dependent):**	$t = 0.07 \times R$
• **Empirical double-corner filter:**	applied
• H normalization:	by acceleration
-Path:	
• **Geometrical spreading**:	$G(R) = R^{-1}$
• **Anelastic attenuation**:	$Q(f) = \max(40, 135 f^{0.76})$
• Shear-wave velocity:	$\beta = 3.7$ km/s
• Density:	2.8 gm/cm^3
-Site:	
• **Site and crustal amplification:**	Ghofrani et al., (2013) for 760 m/s
• **Kappa**:	platform-specified (Niigata: $\kappa = 0.03$ s, Tottori: $\kappa = 0.02$ s)

▲ **Figure 3.** Input parameters applied for Japan.

that both are implemented by multiplying the subsource spectrum by a frequency-dependent function.

Propagation Path Parameters, $P(f)$

The attenuation of ground motion from the subsource to the observation point includes two components.

1. *Geometrical spreading term:* Geometric spreading is a frequency-independent reduction of the entire spectrum based on the distance from the center of the subsource to the observation point (R). EXSIM utilizes a multisegment geometrical spreading function. To specify this function, the user inputs the number of segments, distance ranges of each segment in kilometers, and the exponents of R in each distance range. These parameters are region specific and usually derived empirically. The simplest such model is to specify R^{-1} over all distances, which would correspond to body-wave spreading in a uniform whole space. Another common model is R^{-1} to a transition distance (e.g., 50 km), then $R^{-0.5}$ beyond, where the lower exponent at larger distance represents a transition to surface-wave spreading.
2. *Anelastic attenuation:* The anelastic attenuation parameter provides frequency-dependent attenuation of the subsource spectrum, of the form $\exp(-\gamma(f)R)$, in which $\gamma(f)$ is defined from the Q factor by equation (5). In EXSIM, this has the form $Q(f) = \max(Q_{\min}, Q_0 f^{\eta})$, for which the user specifies $Q_{\min}$, Q_0, and η. $Q_{\min}$, Q_0, and η parameters are region specific and are usually derived empirically.

Site-Response Parameters, Site(f)

The site response in EXSIM is modeled using two frequency-dependent filters:

1. $D(f)$ is the high cut filter function that models the effects of kappa (κ_0, the value of kappa at zero distance;

-Source:

- Magnitude: platform-specified
- Fault geometry, hypocenter: platform-specified
- Slip model: random
- Slip model seed: platform-specified
- Subsource size: $1.6\,\text{km} \times 1.6\,\text{km}$
- **Stress parameter:** $55h + 175$ bars (where h is hypocentral depth)
- Subsource window: Saragoni–Hart ($W_\varepsilon = 0.2$, $W_\eta = 0.2$)
- V_{rup}/V_S : 0.8
- Risetime: $1/f_0$ (~inverse of subsource corner frequency)
- Pulsing%: 50%
- **Subsource duration (distance dependent):**

$$t = \begin{cases} 0 & R \le 10\,\text{km} \\ 0.16 \times (R\text{-}10) & 10 < R \le 70\,\text{km} \\ 9.6 - 0.03 \times (R\text{-}70) & 70 < R \le 130\,\text{km} \\ 7.8 + 0.04 \times (R\text{-}130) & 130 < R \end{cases}$$

- **Empirical double-corner filter:** not applied
- H normalization: by acceleration

-Path:

- **Geometrical spreading**:

$$G(R) = \begin{cases} R^{-1.3} & R \le 50\,\text{km} \\ R^{-0.5} & R > 50\,\text{km} \end{cases}$$

- **Anelastic attenuation**: $Q(f) = \max(500, 525 f^{0.45})$
- Shear-wave velocity: $\beta = 3.7$ km/s
- Density: 2.8 gm/cm^3

-Site:

- **Site and crustal amplification:** Atkinson and Boore (2006) for 1000 m/s
- **Kappa**: platform-specified ($\kappa = 0.005$ s)

▲ **Figure 4.** Input parameters applied for central and eastern North America.

see Anderson and Hough, 1984) or f_{max} (Hanks, 1982). f_{max} or κ_0 are region-specific empirical parameters that represent near-surface attenuation at high frequencies for the reference site condition.

2. $CA(f)$ is the crustal and site amplification factor. This frequency-dependent function is the product of amplification through the regional velocity gradient and amplification due to the near-surface materials at the site (Boore and Joyner, 1997).

Additional Empirical Filter

The input to EXSIM includes one additional frequency-dependent filter that modifies the subsource spectrum. This filter is specified by the user and could serve any number of purposes, such as applying an instrument-response function or an additional site-response function. It may also be used to provide an empirical source parameter filter to model any modifications to the Brune-model spectrum of subsources.

EXSIM INTERNAL RULES

EXSIM follows a number of key internal rules that govern the simulation process. These are summarized in this section, with further details as described by Motazedian and Atkinson (2005), Atkinson *et al.* (2009), and Boore (2009).

Normalization of Subsource Spectra

The normalization of the amplitudes of the subsource spectra is based on the principle of conserving energy at high frequencies (so that amplitudes do not depend on the number of subsources that are summed). The normalization of subsource spectra is based on equations (6) and (7); this is an acceleration-based normalization.

Dynamic Subsource Corner Frequency

The concept of the dynamic corner frequency is that the frequency content of the simulated motions should decrease as the rupture grows, until the ruptured area reaches a prescribed ratio of fault area. This concept is implemented by decreasing the corner frequency of subsources (f_{0i}). Each subsource is initiated when the rupture front reaches its center, and its corner frequency is given by

$$f_{0i} = 4.9 \times 10^6 \beta \left(\frac{N \times \Delta\sigma}{N_R \times M_0} \right)^{1/3}, \quad (8)$$

in which N_R is the number of fractured subsources when the rupture front reaches the ith subsource and the rest of the parameters are those introduced in equations (3) and (7). The result of this algorithm is that the low-frequency spectral content increases as the rupture progresses; this balances the ratio of high- to low-frequency content.

Double-Corner Empirical Source Filter

For earthquakes in California, we use the additional empirical filter to mimic the empirical observation of a spectral sag near the corner frequency for large events, which produces an apparent double-corner source spectrum, as illustrated in Figure 1. The double-corner shape is a function of magnitude as prescribed by Atkinson and Silva (1997), with the depth of the sag relative to the Brune model increasing with magnitude. The application of the empirical filter improves goodness of fit of the simulations at longer periods for earthquakes in California.

PARAMETERS FOR SCEC BBP VALIDATION

There are three region-based sets of EXSIM input parameters that have been implemented for the platform validations exercises, for California, Japan, and ENA, as summarized in Figures 2–4. Many of the source parameters are set by the platform and are not region specific. Parameters in bold font are

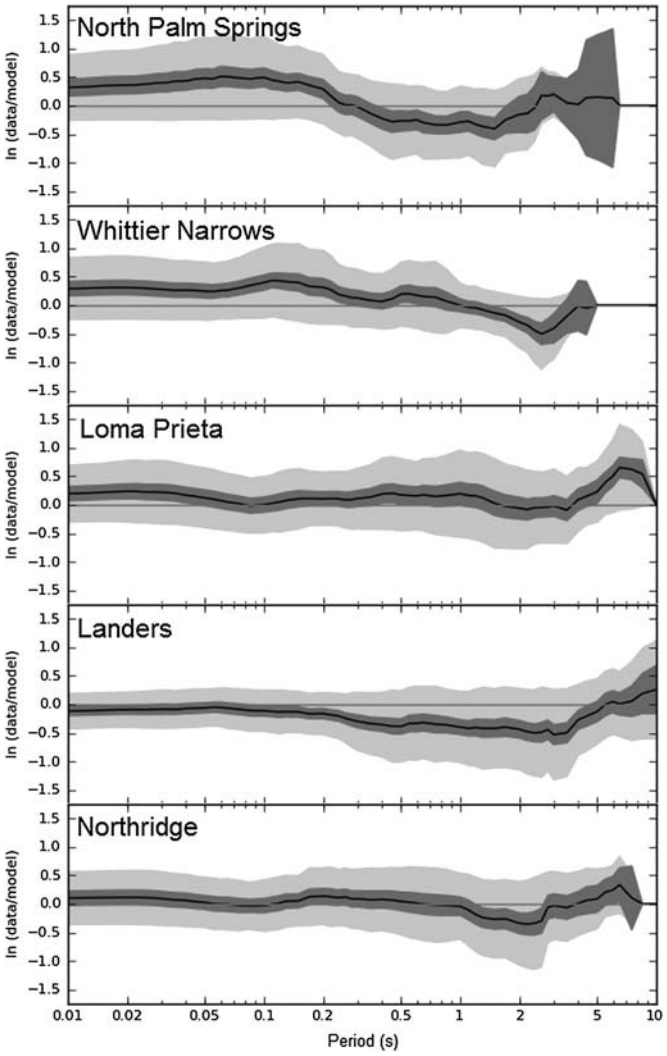

▲ **Figure 5.** Goodness-of-fit plots of five California earthquakes' simulations using extended finite-fault simulation (EXSIM) on Broadband Platform (BBP) V14.3. The black line is mean bias, light gray shading shows its standard deviation, and dark shading shows 90% confidence limits on the mean bias.

the important region-specific parameters that typically differ from one region to another. Ⓔ The electronic supplement to this article gives the input files to EXSIM for each of these applications.

VALIDATION EXERCISES FOR EXSIM

Using the input parameters given in the tables for each region, we simulated 50 random time histories for seven California events, two Japan events, and three ENA events at the observation points specified by the validation exercise, using the magnitudes, fault geometry, and reference site condition as specified by the validation exercise (in Goulet *et al.*, 2015). We compared the spectra of the simulated time histories to those of the recorded time series, using the standard evaluation metrics as specified by the validation exercise. These metrics cover the 0.01 to 10 s period range (fixed by the broadband platform exercise). The spectra of the simulated records was also compared to the predictions of GMPEs for selected magnitudes and distances. In the following, we show the goodness-of-fit results for EXSIM for these validation exercises.

Goodness of Fit for Events in Active Tectonic Regions

As shown in Figure 5, on average EXSIM reproduces the observed pseudoacceleration (5% damped response spectra) for California events with relatively low bias (< factor of

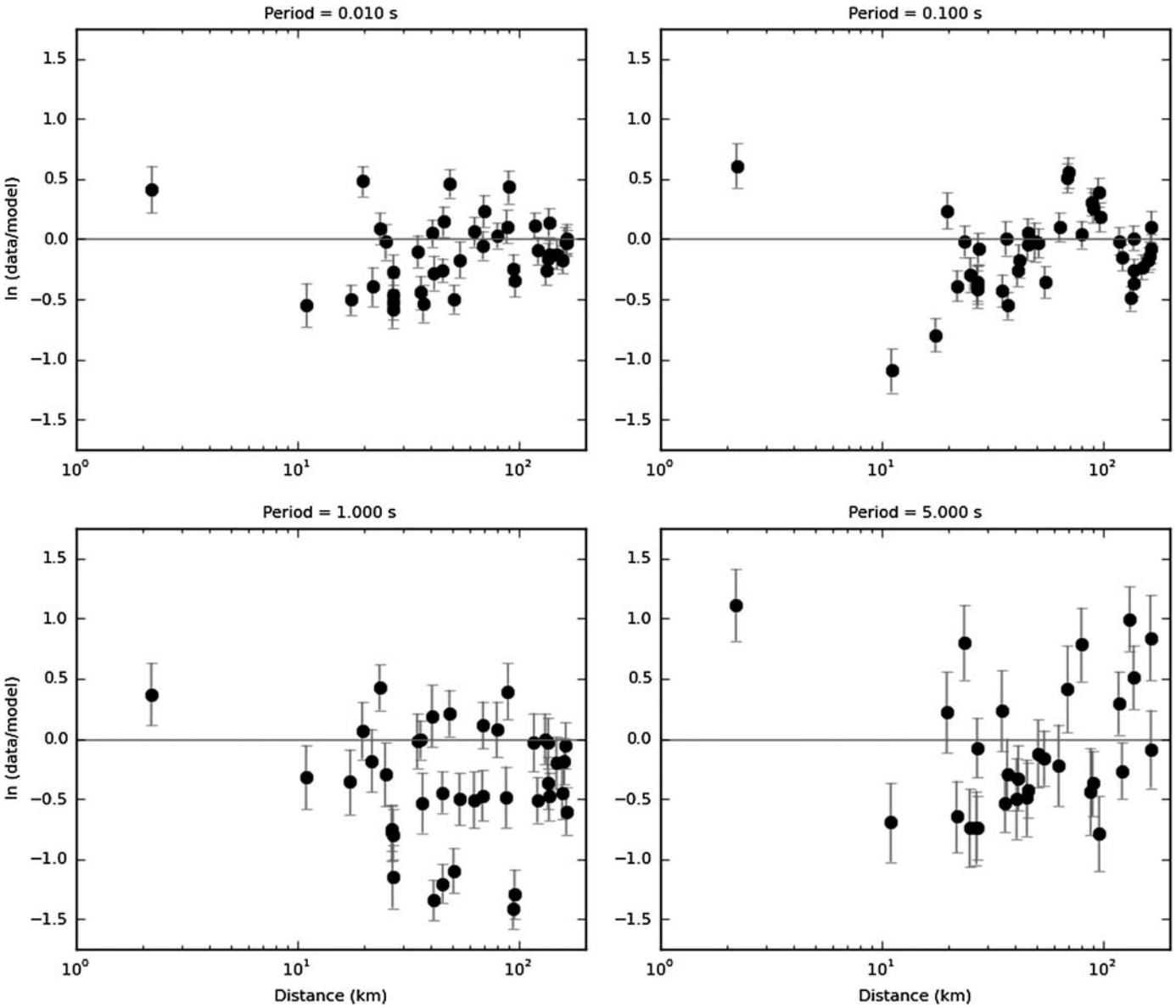

▲ **Figure 6.** Goodness of fit of 50 Landers earthquake simulations in four periods as a function of distance, showing mean and standard deviation of residuals over the 50 simulations.

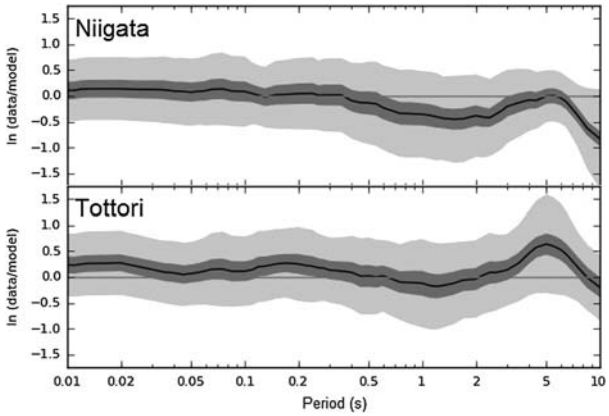

▲ **Figure 7.** Goodness-of-fit plots of two Japan earthquakes' simulations using EXSIM on BBP V14.3. The black line is mean bias, light gray shading shows its standard deviation, and dark shading shows 90% confidence limits on the mean bias.

1.5) over periods from 0.01 to 5 s. The fit tends to be best at short-to-intermediate periods (<2 s). It could be further improved using an event-specific stress parameter to remove the residual short-period bias on an event-by-event basis. However, the event-specific stress is not predictable in advance of an event.

An example of residual trends with distance is shown in Figure 6 for the Landers event. Overall the attenuation model is satisfactory, considering it is based on an average regional model and does not account for details of crustal structure and their event-specific effects on wave propagation.

Japan Events

The overall bias for Japan events is similar to that for California, as illustrated in Figures 7 and 8.

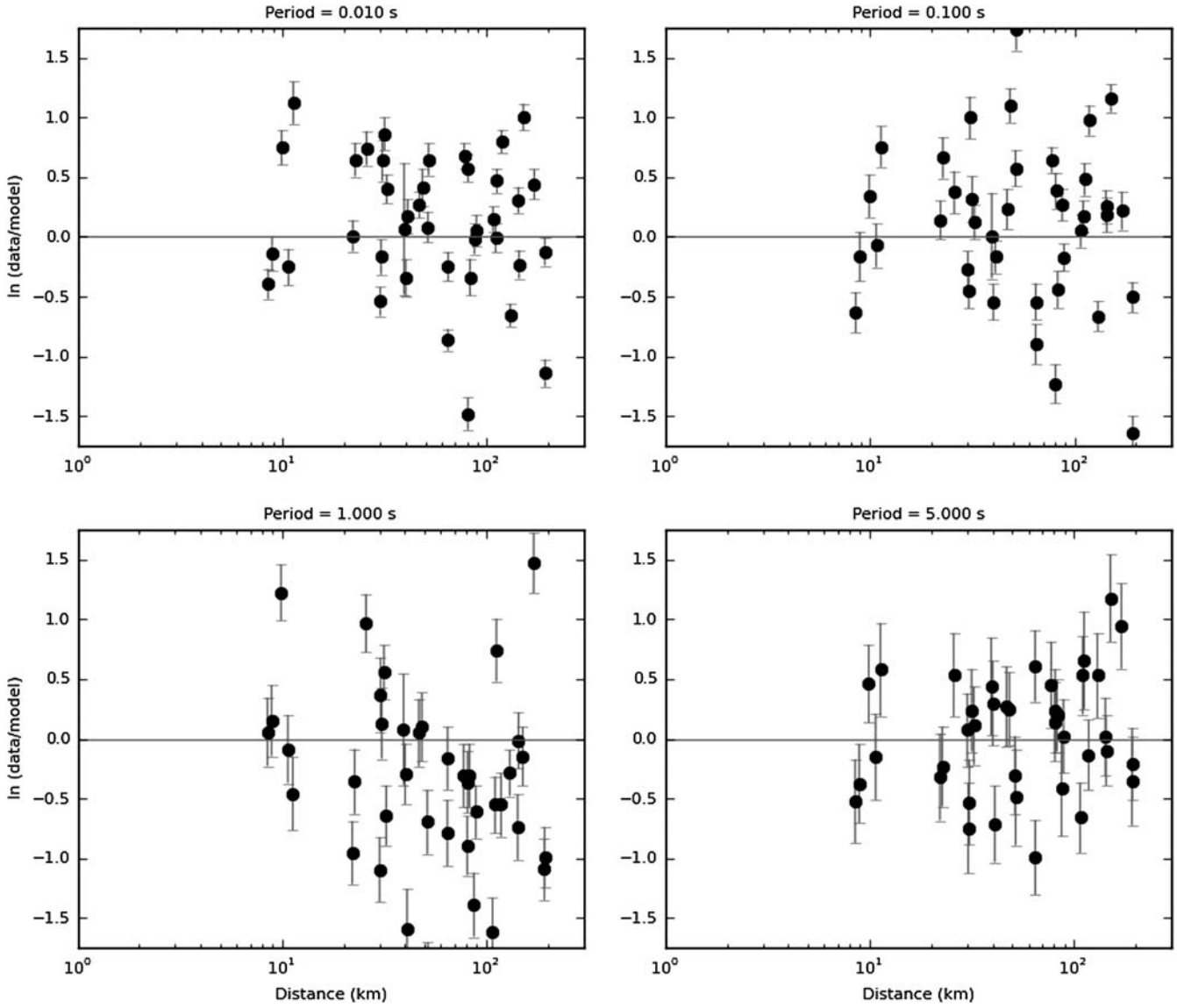

▲ **Figure 8.** Goodness of fit of 50 Niigata earthquake simulations in four periods as a function of distance.

Comparison of EXSIM Predictions to GMPEs

Figure 9 compares the average spectral accelerations predicted by EXSIM to those from the Next Generation Attenuation-West 1 GMPEs, considering two scenarios. Overall, the EXSIM predictions and the GMPEs agree well, with the EXSIM predictions falling within the defined acceptance criteria as given by Goulet *et al.* (2015).

Eastern North America

Validation of the EXSIM model for ENA events is challenging and subject to larger uncertainties, due to the sparse data used in the validation exercise. To provide the best fit for the sparse data, we utilized a depth-dependent stress drop in ENA, based on fitting the best stress of these events as a function of focal depth; such a function has been suggested by J. Boatwright (personal comm., 2013). The model uses a stress near 600 bars for shallow events (~8 km), increasing to a stress near 1500 bars for deep events (~25 km). As shown in Figure 10, motions at periods <2 s (which is the period range over which stochastic methods are expected to perform well) are predicted with relatively low bias for the **M** 5 Riviere de Loup and **M** 5.8 Mineral earthquakes (shallow events), whereas the ground motions from the **M** 5.8 Saguenay earthquake (a deep event) are larger than predicted, despite the high assumed stress. The high ground-motion amplitudes for Saguenay, at short periods, are a well-known conundrum in ENA seismology (e.g., Boore and Atkinson, 1992). Figure 11 shows a typical plot of ground-motion residuals as a function of distance.

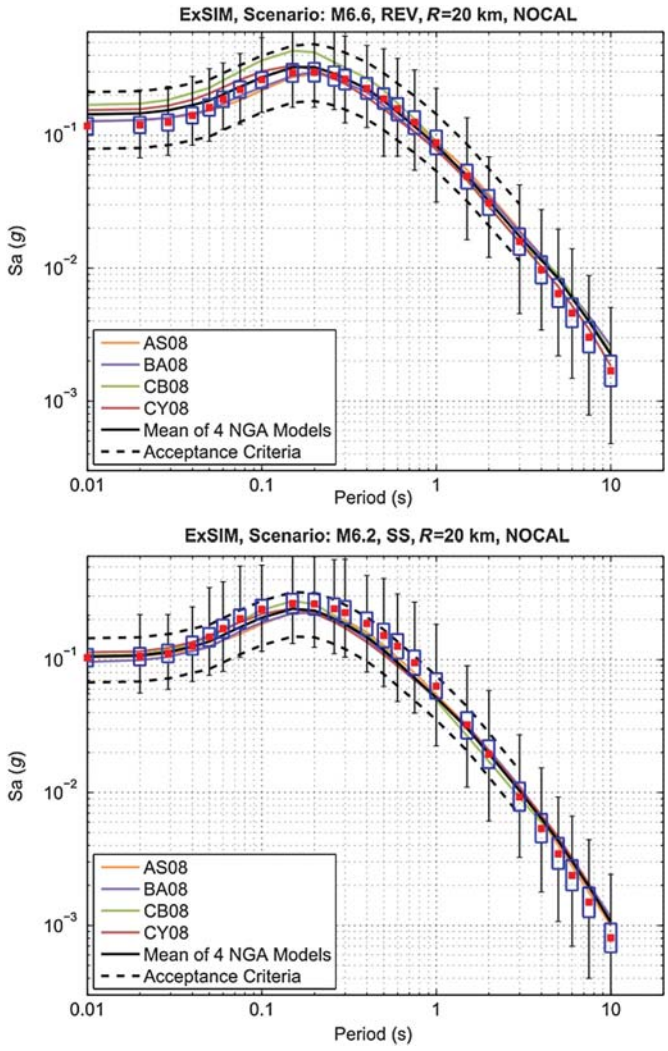

▲ **Figure 9.** Comparison of the mean of EXSIM spectral accelerations (symbols, with box showing ±1 standard deviation, and total length of error bars indicating minimum and maximum values) with predictions of four Next Generation Attenuation-West 1 (NGA-W1) ground-motion prediction equations. The dashed lines show the acceptance criteria (Goulet *et al.*, 2015).

Summary of Goodness-of-Fit

Table 1 provides an overall summary of the goodness of fit for all of the events studied, grouped by distance range (where data are available). For each indicated range, the average residual (observed/predicted, in ln units) is given. The table is shaded to allow an event-by-event visual scan of period and distance ranges where the method performs well (light gray), marginally (white), or poorly (dark gray) (see Goulet *et al.*, 2015). Overall, the method performs remarkably well, considering its simplicity and the limitation of the exercises performed here; we note

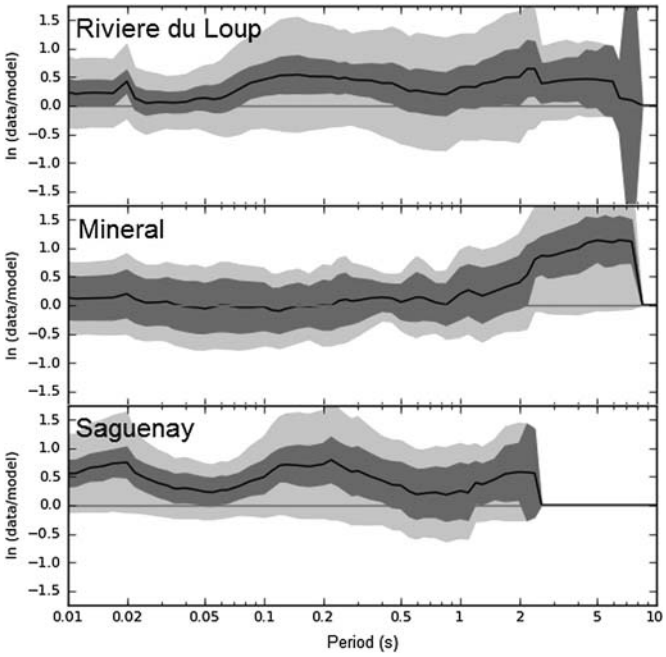

▲ **Figure 10.** Goodness-of-fit plots of three eastern North America earthquakes' simulations using EXSIM on BBP V14.3. The black line is mean bias, light gray shading shows its standard deviation, and dark shading shows 90% confidence limits on the mean bias.

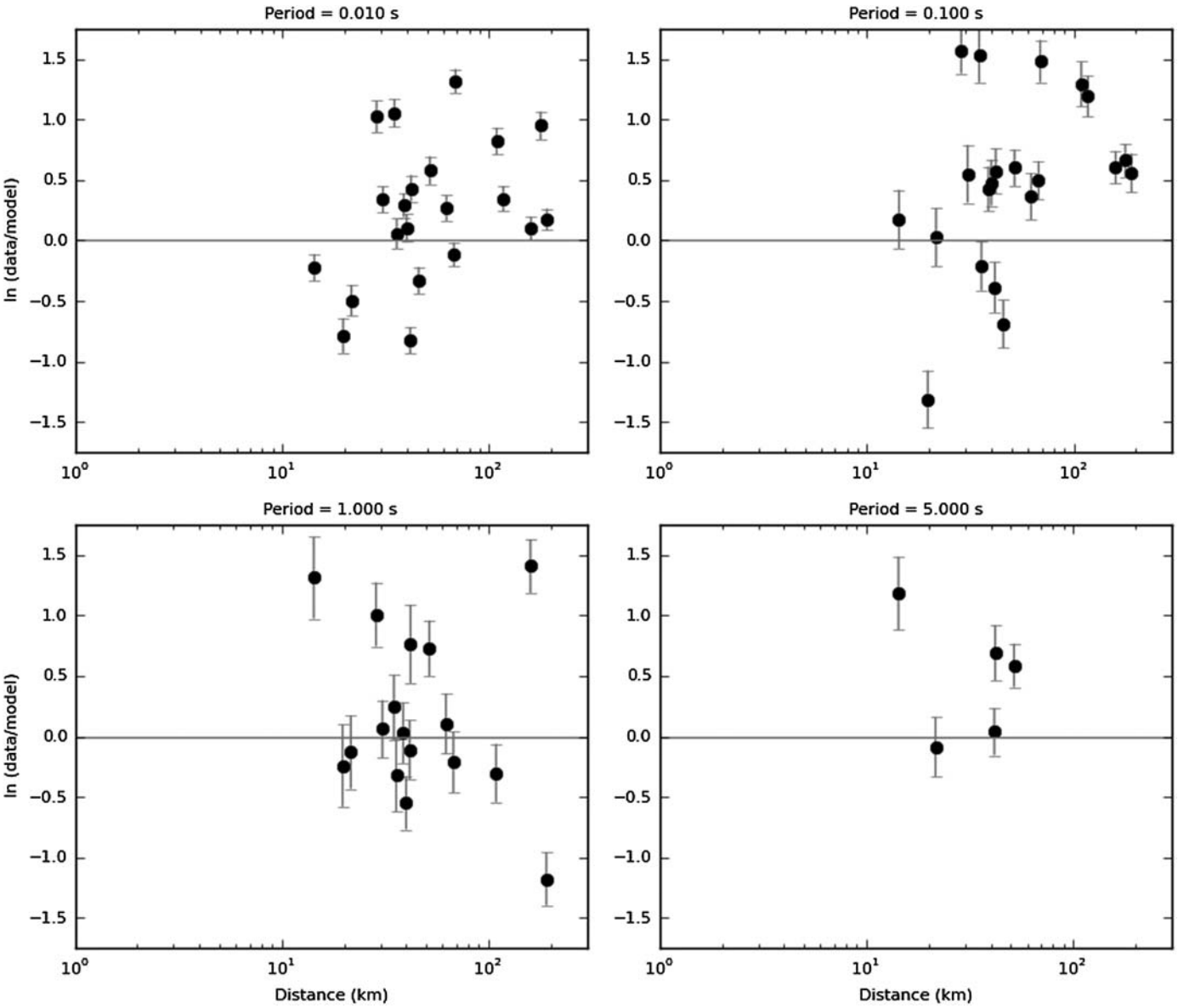

▲ **Figure 11.** Goodness of fit of 50 Riviere du Loup earthquake simulations in four periods as a function of distance.

that the fit could be further improved by optimizing the input parameters in a more comprehensive way. Such optimization was beyond the scope of this study.

SUMMARY AND CONCLUSIONS

EXSIM is a stochastic finite-fault algorithm to simulate ground motions that uses simple semiempirical functions to represent average earthquake source, path, and site effects. A key advantage of EXSIM is that it requires limited knowledge of the specifics of source and path effects, which may be poorly known for future events. Despite its simplicity, EXSIM works remarkably well at reproducing average spectral amplitudes in a variety of settings, over a broad range of magnitudes, distances, and periods.

ACKNOWLEDGMENTS

EXSIM has benefitted in both coding and improving the algorithm from the efforts of several collaborators over the years, including Igor Beresnev, Dariush Motazedian, and David Boore. The EXSIM code reflects their work, as well as that of the authors. Financial support for this work was provided by the Southern California Earthquake Center (SCEC), Next Generation Attenuation-East (NGA-East), and Natural Sciences and Engineering Research Council of Canada. We thank

Table 1
Goodness-of-Fit Summary

	Event (M_w, Mech.)	PSA[0.01s–0.1s]		PSA]0.1s–1.0s]		PSA]1.0s–3.0s]		PSA>3.0s	
R_{rup} = [0–5] km	Chino Hills (5.39, ROBL)								
	Alum Rock (5.45, SS)	**–1.04**	**1.04**	**–1.15**	**1.15**	**–1.15**	**1.15**	**–0.96**	**0.96**
	Whittier Narrows (5.89, REV)								
	North Palm Springs (6.12, ROBL)	**0.38**	**0.38**	**0.15**	**0.31**	**0.20**	**0.20**	**–0.08**	**0.08**
	Tottori (6.59, SS)	**–1.18**	**1.18**	**–0.19**	0.63	**–0.17**	**0.21**	**–0.23**	**0.23**
	Niigata (6.65, REV)								
	Northridge (6.73, REV)								
	Loma Prieta (6.94, ROBL)	**0.19**	**0.38**	**0.20**	**0.37**	**0.48**	**0.97**	**0.09**	0.58
	Landers (7.22, SS)	**0.73**	**0.73**	**0.28**	**0.28**	0.61	0.61	**1.13**	**1.13**
	Riviere-du-Loup (4.6 REV)								
	Mineral (5.68 REV)								
	Saguenay (5.81 REV)								
	Average CA	**0.11**	0.55	**–0.02**	**0.47**	**0.18**	**0.81**	**0.26**	**0.81**
	Average CENA								
	Average ALL	**–0.08**	0.64	**–0.04**	**0.50**	**0.13**	**0.73**	**0.16**	0.70
R_{rup} = [5–20] km	Chino Hills (5.39, ROBL)	**0.21**	**0.32**	**0.33**	**0.44**	0.64	0.64	**0.80**	**0.80**
	Alum Rock (5.45, SS)	**–0.28**	**0.35**	**–0.16**	**0.40**	**0.25**	0.51	0.63	**0.78**
	Whittier Narrows (5.89, REV)	**0.23**	**0.32**	**0.23**	**0.40**	**–0.14**	**0.28**	**–0.35**	**0.38**
	North Palm Springs (6.12, ROBL)	**0.08**	**0.38**	**–0.13**	**0.40**	**–0.08**	**0.44**	**0.02**	0.56
	Tottori (6.59, SS)	**–0.46**	**0.47**	**–0.03**	**0.38**	**0.02**	**0.39**	**0.32**	**0.41**
	Niigata (6.65, REV)	**0.16**	0.52	**0.29**	**0.49**	**–0.16**	0.52	**–0.22**	**0.46**
	Northridge (6.73, REV)	**0.23**	**0.38**	**0.30**	**0.45**	**0.23**	0.54	**0.30**	**0.42**
	Loma Prieta (6.94, ROBL)	**0.33**	**0.40**	**0.22**	**0.39**	**–0.12**	**0.36**	**0.19**	**0.47**
	Landers (7.22, SS)	**–0.29**	0.57	**–0.12**	0.52	**–0.40**	**0.45**	**–0.29**	0.53
	Riviere-du-Loup (4.6 REV)	–0.62	0.63	**0.12**	**1.04**	0.64	**1.03**	**1.14**	**1.14**
	Mineral (5.68 REV)	**–0.46**	**0.46**	**–0.17**	**0.23**	**0.20**	**0.20**	**0.28**	**0.28**
	Saguenay (5.81 REV)								
	Average CA	**0.15**	**0.37**	**0.15**	**0.42**	**0.08**	**0.45**	**0.31**	0.56
	Average CENA	–0.57	0.57	**0.03**	**0.77**	**0.47**	0.70	**0.93**	**0.93**
	Average ALL	**0.06**	**0.40**	**0.14**	**0.43**	**0.07**	**0.46**	**0.25**	0.52

(Continued next page.)

Table 1 (continued)
Goodness-of-Fit Summary

	Event (M_W, Mech.)	PSA[0.01s–0.1s]		PSA]0.1s–1.0s]		PSA]1.0s–3.0s]		PSA>3.0s	
R_{rup}=[20–70] km	Chino Hills (5.39, ROBL)	**0.26**	0.52	**0.15**	**0.50**	**0.36**	0.55	0.61	0.67
	Alum Rock (5.45, SS)	**–0.73**	**0.80**	**–0.77**	**0.83**	–0.58	0.67	**0.03**	**0.41**
	Whittier Narrows (5.89, REV)	**0.31**	**0.49**	**0.20**	**0.50**	**–0.22**	**0.37**	**0.06**	**0.22**
	North Palm Springs (6.12, ROBL)	0.56	0.67	**0.07**	0.55	**–0.35**	0.53	**0.34**	**0.34**
	Tottori (6.59, SS)	**0.21**	**0.41**	**–0.13**	0.54	**–0.41**	0.58	**–0.01**	**0.38**
	Niigata (6.65, REV)	**0.16**	**0.46**	**–0.02**	0.55	**–0.43**	0.61	**–0.31**	**0.49**
	Northridge (6.73, REV)	**–0.10**	**0.30**	**–0.17**	**0.39**	–0.55	0.58	**–0.26**	**0.43**
	Loma Prieta (6.94, ROBL)	**–0.11**	**0.39**	**–0.10**	**0.43**	**–0.22**	0.51	**0.30**	**0.48**
	Landers (7.22, SS)	**–0.17**	**0.27**	**–0.31**	**0.43**	–0.64	0.70	**–0.29**	0.53
	Riviere-du-Loup (4.6 REV)	**0.22**	**0.50**	**0.40**	0.66	**0.37**	0.53	**0.24**	**0.32**
	Mineral (5.68 REV)	0.70	0.70	**–0.02**	0.61	0.58	**1.34**	**1.35**	**1.35**
	Saguenay (5.81 REV)	0.57	0.58	–0.58	0.60	**–1.46**	**1.46**		
	Average CA	**0.03**	**0.50**	**–0.11**	0.52	**–0.30**	0.57	**0.02**	0.51
	Average CENA	**0.31**	0.53	**0.25**	0.65	**0.39**	0.66	**0.37**	**0.44**
	Average ALL	**0.08**	**0.49**	**–0.07**	0.53	**–0.28**	0.58	**-0.05**	**0.47**
R_{rup}=[70–300] km	Chino Hills (5.39, ROBL)	**0.46**	0.61	**0.27**	0.59	**0.20**	0.67	**0.47**	**0.83**
	Alum Rock (5.45, SS)	**–0.72**	**0.86**	**–0.83**	**0.95**	**–0.17**	**0.37**	**0.09**	**0.22**
	Whittier Narrows (5.89, REV)								
	North Palm Springs (6.12, ROBL)	**0.08**	**0.22**	**–0.39**	0.52	**–0.45**	**0.46**		
	Tottori (6.59, SS)	**0.48**	0.60	**0.41**	0.64	**0.34**	0.70	**0.74**	**0.87**
	Niigata (6.65, REV)	**0.05**	0.56	**–0.27**	0.61	**–0.39**	0.65	**–0.14**	0.52
	Northridge (6.73, REV)	**0.16**	**0.39**	**0.16**	**0.48**	**–0.83**	**0.88**	–0.56	0.56
	Loma Prieta (6.94, ROBL)	0.61	0.61	0.62	0.65	**0.76**	**0.99**	**0.30**	0.68
	Landers (7.22, SS)	**–0.01**	**0.15**	**–0.28**	**0.37**	**–0.28**	**0.45**	**0.13**	0.53
	Riviere-du-Loup (4.6 REV)	**0.42**	**0.48**	0.54	**0.83**	0.56	**1.12**	**0.97**	**0.97**
	Mineral (5.68 REV)	**–0.07**	0.59	**0.10**	0.53	**0.49**	0.64	**1.08**	**1.08**
	Saguenay (5.81 REV)	**0.42**	0.55	**0.73**	**0.80**	**0.44**	0.60	**–0.12**	**0.12**
	Average CA	**0.04**	**0.50**	**–0.13**	0.60	**–0.03**	0.58	**0.22**	0.56
	Average CENA	**0.26**	0.55	**0.47**	**0.72**	**0.48**	**0.71**	**0.97**	**0.99**
	Average ALL	**0.15**	0.53	**0.05**	0.63	**0.04**	0.63	**0.33**	0.68

	Event (M_W, Mech.)	PSA[0.01s–0.1s]		PSA]0.1s–1.0s]		PSA]1.0s–3.0s]		PSA>3.0s	
Mechanism	Reverse (REV)	**0.17**	**0.46**	**0.13**	0.54	**–0.12**	0.57	**–0.02**	0.53
	Reverse-Oblique (ROBL)	**0.29**	**0.50**	**0.12**	**0.49**	**0.10**	0.57	**0.40**	0.61
	Strike-Slip (SS)	**–0.19**	0.51	**–0.28**	0.58	**–0.26**	0.58	**0.17**	0.56
	Normal (NM)								
Total	**Average CA**	**0.06**	**0.47**	**–0.05**	0.51	**–0.14**	0.55	**0.15**	0.54
	Average CENA	**0.22**	0.54	**0.34**	0.69	**0.44**	0.69	**0.75**	**0.79**
	Average ALL	**0.09**	**0.49**	**0.00**	0.54	**–0.11**	0.57	**0.15**	0.56

In each period range the left number is the mean goodness of fit and right number is the mean absolute goodness of fit. Light gray is a pass, white indicates marginal acceptance, and dark gray is unsatisfactory.

Joe Fletcher and two anonymous reviewers for constructive comments. We also thank our SCEC colleagues for all of their valuable and stimulating collaboration in this project.

REFERENCES

Anderson, J. G., and S. E. Hough (1984). A model for the shape of the Fourier amplitude spectrum of acceleration at high frequencies, *Bull. Seismol. Soc. Am.* **74,** 1969–1993.

Assatourians, K., and G. Atkinson (2012). *EXSIM12: A Stochastic Finite-Fault Computer Program in FORTRAN*, http://www.seismotoolbox.ca (last accessed November 2014).

Atkinson, G. M., and D. M. Boore (2006). Earthquake ground-motion prediction equations for eastern North America, *Bull. Seismol. Soc. Am.* **96,** 2181–2205.

Atkinson, G. M., and W. Silva (1997). An empirical study of earthquake source spectra for California earthquakes, *Bull. Seismol. Soc. Am.* **87,** 97–113.

Atkinson, G. M., D. M. Boore, K. Assatourians, K. Campbell, and D. Motazedian (2009). A guide to differences between stochastic point-source and stochastic finite-fault simulations, *Bull. Seismol. Soc. Am.* **99,** 3192–3201.

Beresnev, I., and G. Atkinson (1998). FINSIM—a FORTRAN program for simulating stochastic acceleration time histories from finite faults, *Seismol. Res. Lett.* **69,** 27–32.

Beresnev, I. A., and G. M. Atkinson (1997). Modeling finite-fault radiation from the ω^n spectrum, *Bull. Seismol. Soc. Am.* **87,** 67–84.

Boore, D. M. (1983). Stochastic simulation of high-frequency ground motions based on seismological models of the radiated spectra, *Bull. Seismol. Soc. Am.* **73,** 1865–1894.

Boore, D. M. (2003). Simulation of ground motion using the stochastic method, *Pure Appl. Geophys.* **160,** 635–675.

Boore, D. M. (2005). *SMSIM—Fortran Programs for Simulating Ground Motions from Earthquakes: Version 2.3—A Revision of OFR 96–80–A*, http://www.daveboore.com/smsim (last accessed August 2014).

Boore, D. M. (2009). Comparing stochastic point-source and finite-source ground-motion simulations: SMSIM and EXSIM, *Bull. Seismol. Soc. Am.* **99,** 3202–3216.

Boore, D. M., and G. M. Atkinson (1992). Source spectra for the 1988 Saguenay, Quebec, earthquakes, *Bull. Seismol. Soc. Am.* **82,** 683–719.

Boore, D. M., and W. B. Joyner (1997). Site amplifications for generic rock sites, *Bull. Seismol. Soc. Am.* **87,** 327–341.

Bour, M., and M. Cara (1997). Test of a simple empirical Green's function method on moderate-sized earthquakes, *Bull. Seismol. Soc. Am.* **87,** 668–683.

Brune, J. N. (1970). Tectonic stress and the spectra of seismic shear waves from earthquakes, *J. Geophys. Res.* **75,** 4997–5009.

Brune, J. N. (1971). Tectonic stress and the spectra of seismic shear waves from earthquakes: Correction, *J. Geophys. Res.* **76,** 5002.

Ghofrani, H., G. Atkinson, and K. Goda (2013). Stochastic finite-fault simulations of the Tohoku, Japan, earthquake, *Bull. Seismol. Soc. Am.* **103,** 1307–1320.

Goulet, C. A., N. A. Abrahamson, P. G. Somerville, and K. E. Wooddell (2015). The SCEC broadband platform validation exercise: Methodology for code validation in the context of seismic hazard analyses, *Seismol. Res. Lett.* **86,** no. 1, doi: 10.1785/0220140104.

Hanks, T. C. (1982). f_{max}, *Bull. Seismol. Soc. Am.* **72,** 1867–1879.

Hartzell, S. H. (1978). Earthquake aftershocks as Green's functions, *Geophys. Res. Lett.* **5,** 1–4.

Irikura, K. (1983). Semi-empirical estimation of strong ground motions during large earthquakes, *Bull. Disast. Prev. Res. Inst.* **33,** 63–104.

Irikura, K. (1992). The construction of large earthquake by a superposition of small events, *Proceedings of the Tenth World Conference on Earthquake Engineering*, Vol. 10, Madrid, Spain, 19–24 July 1992, 727–730.

Irikura, K., and K. Kamae (1994). Estimation of strong ground motion in broad-frequency band based on a seismic source scaling model and an empirical Green's function technique, *Ann. Geofisc.* **37,** 1721–1743.

Leonard, M. (2010). Earthquake fault scaling: Self-consistent relating of rupture length, width, average displacement, and moment release, *Bull. Seismol. Soc. Am.* **100,** no. 5A, 1971–1988.

Motazedian, D., and G. M. Atkinson (2005). Stochastic finite-fault modeling based on a dynamic corner frequency, *Bull. Seismol. Soc. Am.* **95,** 995–1010.

Saragoni, G., and G. Hart (1974). Simulation of artificial earthquakes, *Int. J. Earthq. Eng. Struct. Dynam.* **2,** 249–267.

Schneider, J. F., W. J. Silva, and C. Stark (1993). Ground motion model for the 1989 M 6.9 Loma Prieta earthquake including effects of source, path, and site, *Earthq. Spectra* **9,** 251–287.

Gail M. Atkinson
Karen Assatourians
Department of Earth Sciences
Western University
London, Ontario, Canada N6A 5B7
gmatkinson@aol.com
karenassatourians@yahoo.com

Published Online 17 December 2014